15th Australasian Fluid Mechanics Conference
The University of Sydney, Sydney, Australia
13-17 December 2004

Numerical Analysis of Turbulent Convective Heat Transfer Processes in a Square-Sectioned U-bend Duct

S. Etemad[1] and B. Sundén[2]

[1]Thermodynamic Analysis, Dept 97613,
Volvo Car Corporation, SE-405 31 Gothenburg, SWEDEN
setemad@volvocars.com

[2]Division of Heat Transfer, Lund Institute of Technology, Box 118
SE-221 00 Lund, SWEDEN

Abstract

The flow and thermal field in a square-sectioned 180° U-bend were investigated using five turbulence models, namely Suga's quadratic and cubic low-Re k-ε, V2F k-ε, RSM-EVH and RSM-GGDH. All models managed to mimic the general flow and thermal patterns. The V2F-version used in this study, however, over-predicted the pressure-induced secondary flow and seems to need modifications and/or re-tuning of the coefficients to reduce its redistribution of turbulence energy. Suga's two k-ε variants are less CPU-demanding and perform relatively well and, hence are interesting candidates for industrial applications. The RSM models performed best.

Introduction

The turbulent flow and heat transfer in square-sectioned 180° U-bends give rise to complex three-dimensional motion and heat transfer phenomena which are similar to the phenomena that occur frequently in many engineering applications such as cooling passages in gas turbine blades and automobile engines. The study of generic cases like the U-bend is hence important for the understanding of the flow and heat transfer mechanisms in the industrial applications mentioned above. In the present study the published experimental data [8] were used for the validation of the results for a square-sectioned U-bend. Besides the interest in studying the complex flow and heat transfer phenomena, the other objective for this work is to explore the performance of the methods for accurate prediction of flow-heat transfer behaviour in such generic cases for final use in engineering applications.

Problem Description

The geometry is a square-sectioned 180° U-bend duct with the side length D=88.9 mm. The bend mid-line radius, r, was 3.35D as illustrated in figure 1. The Reynolds number was $Re_D=U_mD/\nu$=56000 where U_m=9.11 m/s is the mean velocity. The Dean number was $De=Re_D\sqrt{(D/2r)}^{0.5}$=21634 (where ν is the kinematic viscosity). The bend was provided with a long straight inlet part and a 4.5D straight outlet part as shown in figure 1b. As specified in table 1 the inlet length was tuned for each turbulence model to match the flow conditions at -2.2D (upstream the bend) to the ones measured by Johnson and Launder [8]. As shown in figure 1(a), the cross-section grid consisting of 51x51 grid points expanded from a fine near-wall grid to a coarser off-wall grid. The mean Y^+ was nearly 7 ($Y^+=Yu_\tau/\nu$ where $u_\tau=\sqrt{(\tau_w/\rho)}^{0.5}$ is the friction velocity, ρ is the density and $\tau_w=(\rho\nu\partial U/\partial y)_{at\ y=0}$ is the wall shear stress). Hence, the grid was compromised to be used for both high- and low-Re models. The grid details appear in table 1. As inlet boundary condition constant temperature, 20°C, and uniform velocity profile was used. Constant heat flux was used on walls.

Turbulence Model	Grid points (Streamwise) inlet+bend+outlet	Inlet length	mean Y^+	Y^+ range
Suga, Quad	179+91+41	20D	6.8	0-11
Suga, Cubic	179+91+41	20D	6.8	0-11
V2F	241+91+41	28D	6.1	0-11
RSM, EVH	286+91+41	32D	7.5	0-14
RSM, GGDH	286+91+41	32D	7.6	0-14

Table 1. Grid specifications.

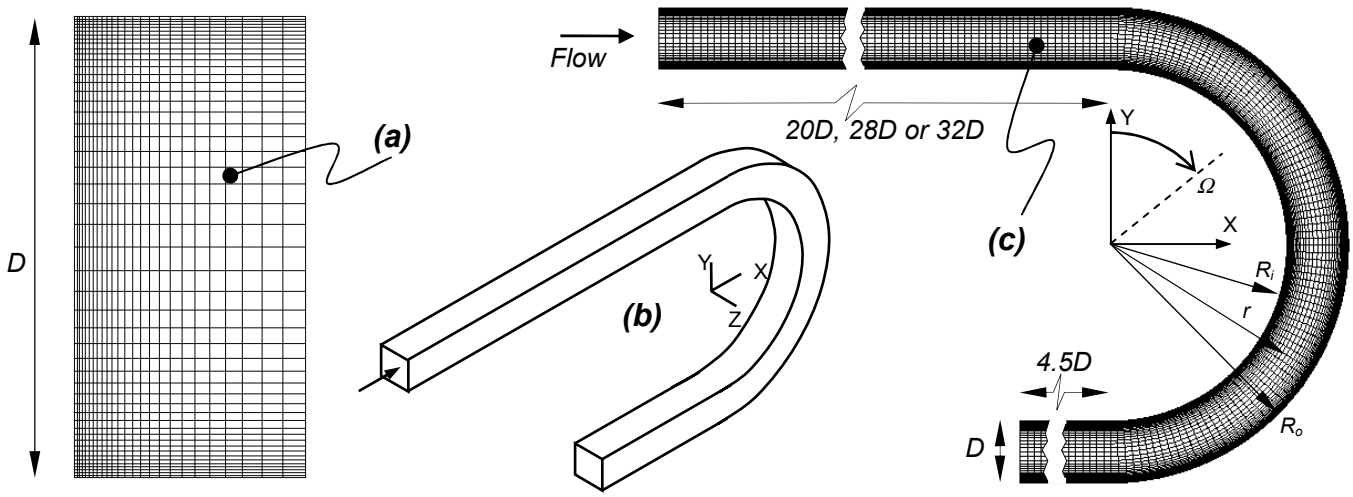

Figure 1. (a) Half of the cross-section mesh, (b) Bend and its co-ordinate system, (c) Streamwise mesh.

Turbulence Models

The turbulence models used in this work are Suga's quadratic and cubic low-Re k-ε [1-2], V2F k-ε [4,7] and two versions of RSM [9], Reynolds stress model, namely isotropic EVH [10] and anisotropic GGDH [3] (i.e. Eddy Viscosity Hypothesis and Generalised Gradient Diffusion Hypothesis, respectively). The models are briefly explained below. To obtain non-linear eddy viscosity models, like Suga's quadratic and cubic model, and thereby account for the non-isotropic nature of the turbulence, series expansions of functional terms are added to the linear eddy viscosity model (Boussinesq assumption). The general expression for the Reynolds stresses, $-\rho\overline{u_i u_j}$, is given below.

$$\rho\overline{u_i u_j} = \frac{2}{3}\rho k\delta_{ij} - 2\mu_t S_{ij} + \\ + 4C_1\mu_t\tau(S_{ik}S_{kj} - \frac{1}{3}S_{kl}S_{kl}\delta_{ij}) + 4C_2\mu_t\tau(W_{ik}S_{kj} + W_{jk}S_{ki}) + 4C_3\mu_t\tau(W_{ik}W_{jk} - \frac{1}{3}W_{kl}W_{kl}\delta_{ij}) \\ + 8C_4\mu_t\tau^2(S_{ki}W_{lj} + S_{kj}W_{li})S_{kl} + 8C_5\mu_t\tau^2(S_{kl}S_{kl} - W_{kl}W_{kl})S_{ij} \qquad (1)$$

$$S_{ij} = \frac{1}{2}\left(\frac{\partial U_i}{\partial x_j} + \frac{\partial U_j}{\partial x_i}\right) \quad , \quad W_{ij} = \frac{1}{2}\left(\frac{\partial U_i}{\partial x_j} - \frac{\partial U_j}{\partial x_i}\right) \quad , \quad S = \frac{k}{\varepsilon}\sqrt{2S_{ij}S_{ij}} \quad , \quad W = \frac{k}{\varepsilon}\sqrt{2W_{ij}W_{ij}} \qquad (2)$$

Note that X_i=*X,Y,Z* and x_i=*x,y,z* are the streamwise and Cartesian co-ordinates, U_i and u_i are the time averaged and fluctuating velocity, respectively, in x_i-direction and $\tau = k/\varepsilon$ is the turbulent dissipation time scale. The first line in eq. (1) contains only the linear version. By adding the second and the third line containing the quadratic and cubic products of strain and vorticity rate, S_{ij} and W_{ij} , the quadratic and cubic model, respectively, is obtained. The coefficients C_1-C_5 and C_μ, the turbulent viscosity, μ_t , and the damping function , f_μ , (in Suga's model) are given below.

$$\mu_t = f_\mu \frac{C_\mu \rho k^2}{\varepsilon} \quad , \quad f_\mu = 1 - exp\left(-\left(\tilde{R}_t/90\right)^{0.5} - \left(\tilde{R}_t/400\right)^2\right) \qquad (3)$$

$$C_\mu = \frac{0.3}{1+0.35\eta^{1.5}}\left[1 - exp(-0.36\,exp(0.75\eta))\right] \quad , \quad \eta = max(\tilde{S}, \tilde{W}) \qquad (4)$$

$$\tilde{S} = \frac{k}{2\tilde{\varepsilon}}\sqrt{S_{ij}S_{ij}} \quad , \quad \tilde{W} = \frac{k}{2\tilde{\varepsilon}}\sqrt{W_{ij}W_{ij}} \quad , \quad \tilde{R}_t = k^2/(\nu\tilde{\varepsilon}) \qquad (5)$$

C_1= *-0.1*, C_2=*0.1*, C_3=*0.26*, $C_4 = 10.0 \cdot C_\mu^2$ and $C_5 = 5.0 \cdot C_\mu^2$.

In the k-ε models two transport equations, one for the turbulent kinetic energy, *k*, and another one for its dissipation rate, ε, are solved. These are expressed in a condensed general form below.

$$\frac{\partial(\rho k)}{\partial t} + \frac{\partial}{\partial x_j}\left(\rho U_j k\right) = \frac{\partial}{\partial x_j}\left[\left(\mu + \frac{\mu_t}{\sigma_k}\right)\frac{\partial k}{\partial x_j}\right] + P_k - \rho\varepsilon \qquad (6)$$

$$\frac{\partial(\rho\varepsilon)}{\partial t} + \frac{\partial}{\partial x_j}\left(\rho U_j \varepsilon\right) = \frac{\partial}{\partial x_j}\left[\left(\mu + \frac{\mu_t}{\sigma_\varepsilon}\right)\frac{\partial \varepsilon}{\partial x_j}\right] + f_1\frac{C_{\varepsilon 1}}{T_s}P_k - f_2\frac{C_{\varepsilon 2}}{T_s}\rho\varepsilon + E + Y_c \qquad (7)$$

$$P_k = -\rho\overline{u_i u_j}\frac{\partial U_i}{\partial x_j} \quad , \quad \varepsilon = \nu\overline{\frac{\partial u_i}{\partial x_j}\frac{\partial u_i}{\partial x_j}} \quad , \quad T_s = \frac{k}{\varepsilon} \qquad (8)$$

In Suga's model, as can be seen above the *k*-equation has its conventional form while in the ε-equation two terms, *E* and Y_c , expressed below, are added and ε is replaced by $\tilde{\varepsilon}$, as defined below, which is the isotropic part of ε and is zero at the wall. The model coefficients appear in table 3.

$$E = 0.0022\,\tilde{S}\mu_t\frac{k^2}{\tilde{\varepsilon}}\left[\frac{\partial^2 U_i}{\partial x_j \partial x_k}\right]^2 \quad , \quad f_1 = 1 \quad , \quad f_2 = 1 - 0.3\,exp\left(-R_t^2\right) \qquad (9)$$

$$Y_c = max\left[0.83\left(\frac{k^{3/2}}{2.5\tilde{\varepsilon}y} - 1\right)\left(\frac{k^{3/2}}{2.5\tilde{\varepsilon}y}\right)^2\frac{\tilde{\varepsilon}^2}{k}, 0\right] \quad , \quad \tilde{\varepsilon} = \varepsilon - 2\nu\frac{\partial\sqrt{k}}{\partial x_i}\frac{\partial\sqrt{k}}{\partial x_i} \qquad (10)$$

In the V2F model [4,7] an additional transport equation for the wall-normal turbulence intensity, $\overline{v^2}$, and an elliptic equation for the redistribution term, *f* , in the $\overline{v^2}$ -equation, have to be solved. The time scale, T_s , length scale, *L*, and, μ_t , are also give below. No wall function or damping function is used in the V2F model.

$$\frac{\partial\left(\rho\overline{v^2}\right)}{\partial t} + \frac{\partial}{\partial x_j}\left(\rho U_j\overline{v^2}\right) = \frac{\partial}{\partial x_j}\left[\left(\mu + \frac{\mu_t}{\sigma_k}\right)\frac{\partial\overline{v^2}}{\partial x_j}\right] + \rho k f - 6\rho\overline{v^2}\frac{\varepsilon}{k} \qquad (12)$$

$$f - L^2\frac{\partial^2 f}{\partial x_j \partial x_j} = \frac{0.4}{T_s}\left(\frac{2}{3} - \frac{\overline{v^2}}{k}\right) + 0.3\frac{P_k}{k} + \frac{5}{T_s}\frac{\overline{v^2}}{k} \qquad (11)$$

$$f_1 = 1 + 0.045\sqrt{k/\overline{v^2}} \quad , \quad f_2 = 1 \quad , \quad E = Y_c = 0 \qquad (13)$$

$$T_s = max\left(\frac{k}{\varepsilon}, 6\sqrt{\frac{\nu}{\varepsilon}}\right) \quad , \quad L = 0.23\,max\left(\frac{k^{3/2}}{\varepsilon}, 70\frac{\nu^{3/4}}{\varepsilon^{1/4}}\right) \quad , \quad \mu_t = C_\mu\rho\overline{v^2}T_s \qquad (14)$$

Reynolds Stress Models, RSM, solve directly the transport equations for the Reynolds stresses, $-\rho\overline{u_i u_j}$, as expressed below.

$$\frac{\partial\left(\rho\overline{u_i u_j}\right)}{\partial t} + \frac{\partial}{\partial x_k}\left(U_k\rho\overline{u_i u_j}\right) = D_{ij} - \rho\left(\overline{u_i u_k}\frac{\partial U_j}{\partial x_k} + \overline{u_j u_k}\frac{\partial U_i}{\partial x_k}\right) - \frac{2}{3}\delta_{ij}\rho\varepsilon + \Phi_{ij} \qquad (15)$$

For the diffusion term, D_{ij} , two alternative models, the isotropic EVH [10] and the anisotropic GGDH [3] are used. *k* and ε are obtained from eqs. (6-7). However, the diffusion terms in eqs. (6-7), here denoted D_k and D_ε , respectively, are modified as given below in table 2 together with D_{ij} for EVH and GGDH.

EVH	GGDH	eq.#
$D_{ij} = \frac{\partial}{\partial x_m}\left(\frac{\mu_{eff}}{\sigma_k}\frac{\partial\overline{u_i u_j}}{\partial x_m}\right)$	$D_{ij} = 0.22\frac{\rho k}{\varepsilon}\frac{\partial}{\partial x_m}\left(\overline{u_m u_n}\frac{\partial\overline{u_i u_j}}{\partial x_n}\right)$	(16)
$D_k = \frac{\partial}{\partial x_m}\left(\frac{\mu_{eff}}{\sigma_k}\frac{\partial k}{\partial x_m}\right)$	$D_k = \frac{\partial}{\partial x_m}\left(0.22\frac{\rho k}{\varepsilon}\overline{u_m u_n}\frac{\partial k}{\partial x_n}\right)$	(17)
$D_\varepsilon = \frac{\partial}{\partial x_m}\left(\frac{\mu_{eff}}{\sigma_\varepsilon}\frac{\partial\varepsilon}{\partial x_m}\right)$	$D_\varepsilon = \frac{\partial}{\partial x_m}\left(0.18\frac{\rho k}{\varepsilon}\overline{u_m u_n}\frac{\partial\varepsilon}{\partial x_n}\right)$	(18)

Table 2. Diffusion terms in RSM, *k* and ε equations.

For the pressure-strain term, Φ_{ij} , the SSG model [11] is used.

$$\Phi_{ij} = -(C_1\varepsilon + C_1^* P_k)b_{ij} + C_2\varepsilon(b_{ik}b_{kj} - \frac{1}{3}\delta_{ij}b_{km}b_{km}) + (C_3 - C_3^*\Pi_b^{0.5})kS_{ij} + \\ + C_4k(b_{ik}S_{jk} + b_{jk}S_{ik} - \frac{2}{3}\delta_{ij}b_{kl}S_{kl}) + C_5k(b_{ik}W_{jk} + b_{jk}W_{ik}) \qquad (19)$$

$$\mu_{eff} = \mu + 0.09\frac{k^2}{\varepsilon} \quad , \quad b_{ij} = \left(\overline{u_i u_j} - \frac{1}{3}\delta_{ij}\overline{u_k u_k}\right)\frac{1}{\overline{u_k u_k}} \quad , \quad \Pi_b = b_{ij}b_{ij} \qquad (20)$$

C_1=*3.4*, C_1^*=*1.8*, C_2=*4.2*, C_3=*0.8*, C_3^*=*1.3*, C_4=*1.25* and C_5=*0.4*. With the RSM models the logarithmic wall function given below is used for the wall-adjacent cells with E_{wf} =*9.0* and κ=*0.42* .

$$u^+ = (1/\kappa)\,ln(E_{wf}\,Y^+) \quad , \quad u^+ = U_1/u_\tau \qquad (21)$$

For the thermal field the simple eddy diffusivity model, SED, was used in all cases. The turbulent heat fluxes are expressed as

$$\rho\overline{u_j h} = -\frac{\mu_t}{\sigma_h}\frac{\partial h}{\partial x_j} \quad , \ \sigma_h = \text{turbulent Prandtl number} = 0.9 \qquad (22)$$

Model	C_μ	σ_k	σ_ε	$C_{\varepsilon 1}$	$C_{\varepsilon 2}$
Suga	0.09	1.0	1.22	1.44	1.92
V2F	0.22	1.0	1.30	1.40	1.90
RSM	0.09	1.0	1.30	1.44	1.83

Table 3. Model coefficients.

Numerical approach

The governing equations were solved using the implicit finite volume non-staggered solver STAR-CD [12]. The SIMPLE algorithm was used for the pressure-velocity coupling. Based on earlier work by Etemad et al. [5-6], the MARS scheme (2nd order) was chosen for velocities and Upwind (1st order) for other quantities. Constant physical properties were assumed.

Results

The results obtained for all models are condensed in two figures. Figure 2 compares the computed profiles of the streamwise velocity, *U*, and temperature, *T*, with the existing measured data on the symmetry plane for several cross-sections. Note that the predicted profiles for -2.2*D* (upstream the bend), 2.2*D* and 5*D* are compared with the experimental data at -5*D*, 5*D*, and 10*D*,

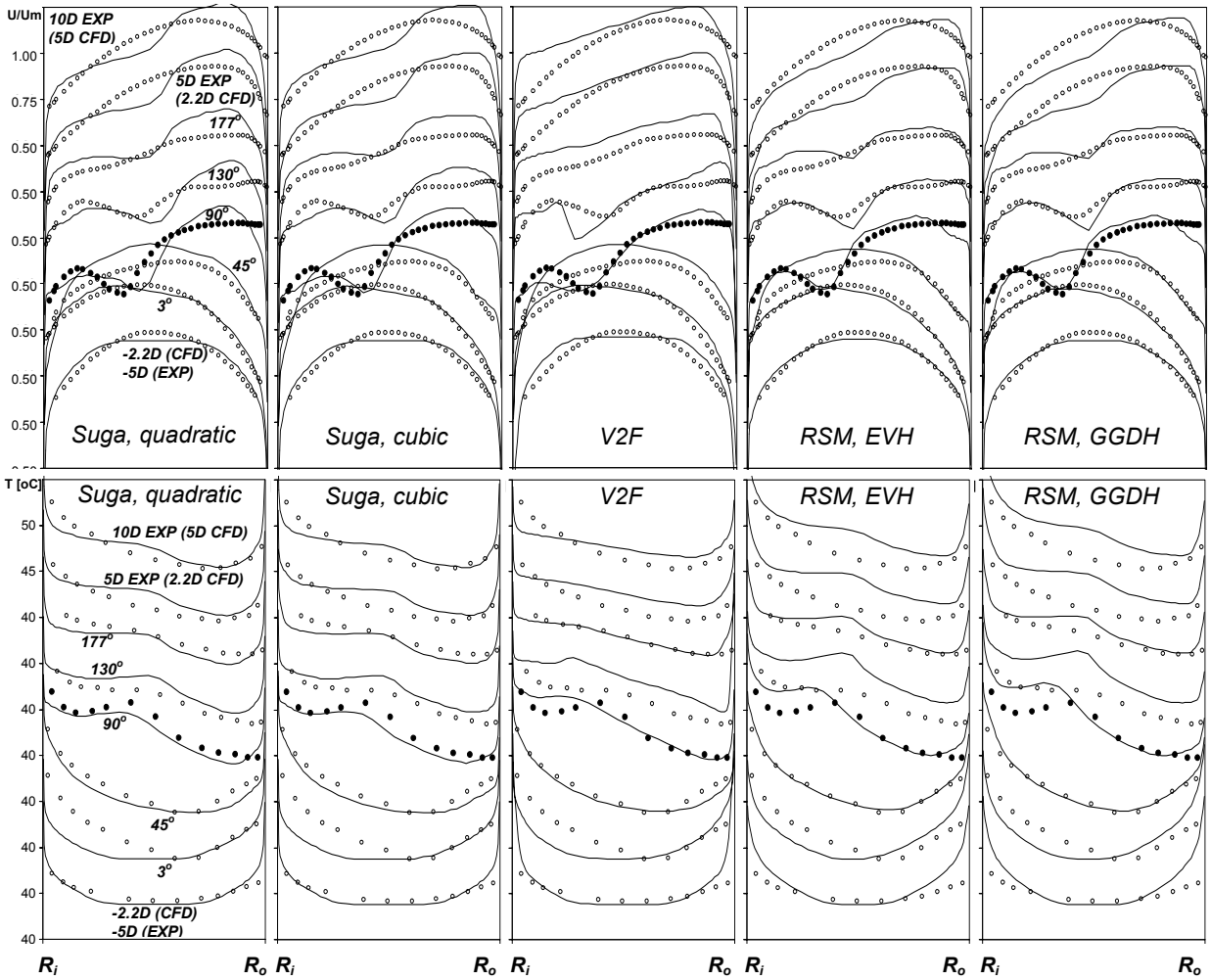

Figure 2. Predicted velocity (top) and temperature (bottom) profiles (lines) on the symmetry plain obtained using Suga's quadratic & cubic model, V2F, RSM-EVH and RSM-GGDH at -2.2*D*, 3°, 45°, 90°, 130°, 177°, 2.2*D* and 4.5*D* and the experimental data (white circles, black only at Ω=90°).

respectively. The diagrams give a quantitative overview of the results. For the understanding of the predicted physical features, however, it is appropriate to review the plots, presented in figure 3 where the vector plots show the pattern of the complex secondary flow in the duct cross-sections together with the mean velocity magnitude contours and isotherms. The first glance at figure 2 shows that at -2.2*D* the velocity profiles are fairly close to the experimental data. This indicates that appropriate inlet length is used for each case. The V2F results, however, differ somewhat from the other models. As it was shown in earlier studies [5-6] the upstream velocity distribution is of great significance for the development of the secondary motion in the bend. Near each side-wall the centrifugal forces, pointing outwards from the bend centre, decrease (due to the friction) and hence, the pressure gradient, which in other regions is in balance with the centrifugal forces, prevails and causes a flow motion near each side-wall towards the bend centre. This initiates the streamwise secondary vortex with a number of smaller satellite-vortices. The velocity distribution upstream the bend dictates the intensity of these vortices which in turn impact the flow and heat transfer in the bend. The V2F prediction of the velocity field upstream the bend deviates most from the other numerical and also experimental data. Hence it is natural to expect that its secondary flow further downstream also deviates most. A closer look at the plots for V2F, especially at 130° in figure 3 implies that this model behaves as the least diffusive among the ones used here. Another general observation is that all models, except V2F, deliver quite similar and reasonable results. It is likely that the V2F version used here needs a re-tuning of coefficients for this kind of flow, because it seems to over-predict the strength and complexity of the secondary flow and might go too far in redistributing the turbulence energy from the streamwise to wall-normal component. The RSM models mimicked the experimental data best, especially at 90° and 130°, (with no significant advantages for GGDH compared to EVH). Suga's cubic model performs slightly better than its quadratic version. This might be due to the fact that the cubic models are known to improve the predictions of curved flow. None of the models seems to mimic the measured velocity profile at 45°. It is likely that this discrepancy is caused by the fact that predicted velocity profiles upstream the bend are more flat than the measured one. It is known that an inviscid flow with a flat velocity profile upstream a bend causes a free-vortex flow in the bend with a higher velocity near the inner radius and lower velocity near the outer radius. Therefore, the predicted velocity profiles in this work at 45° have their peak closer to the inner radius rather than the outer radius (as in the experimental data). When comparing the predicted and measured temperature profiles in figure 2, it should be noted that the temperatures are not normalised and therefore only the shape of these profiles should be considered rather than their level. The general impression is that the temperature profiles correspond well to their velocity counterpart and this indicates the dominating role of the flow field. Except the V2F-results which differ from the rest, all models managed to predict the trends well. Suga's quadratic and cubic models performed similar. Likewise RSM-EVH and RSM-GGDH gave almost the same results. The review of the plots in figure 3 shows that all the used models could capture the complex secondary motions especially at 135°. The most dominating is, however, the main vortex (here counter-clockwise) which convects the cold high

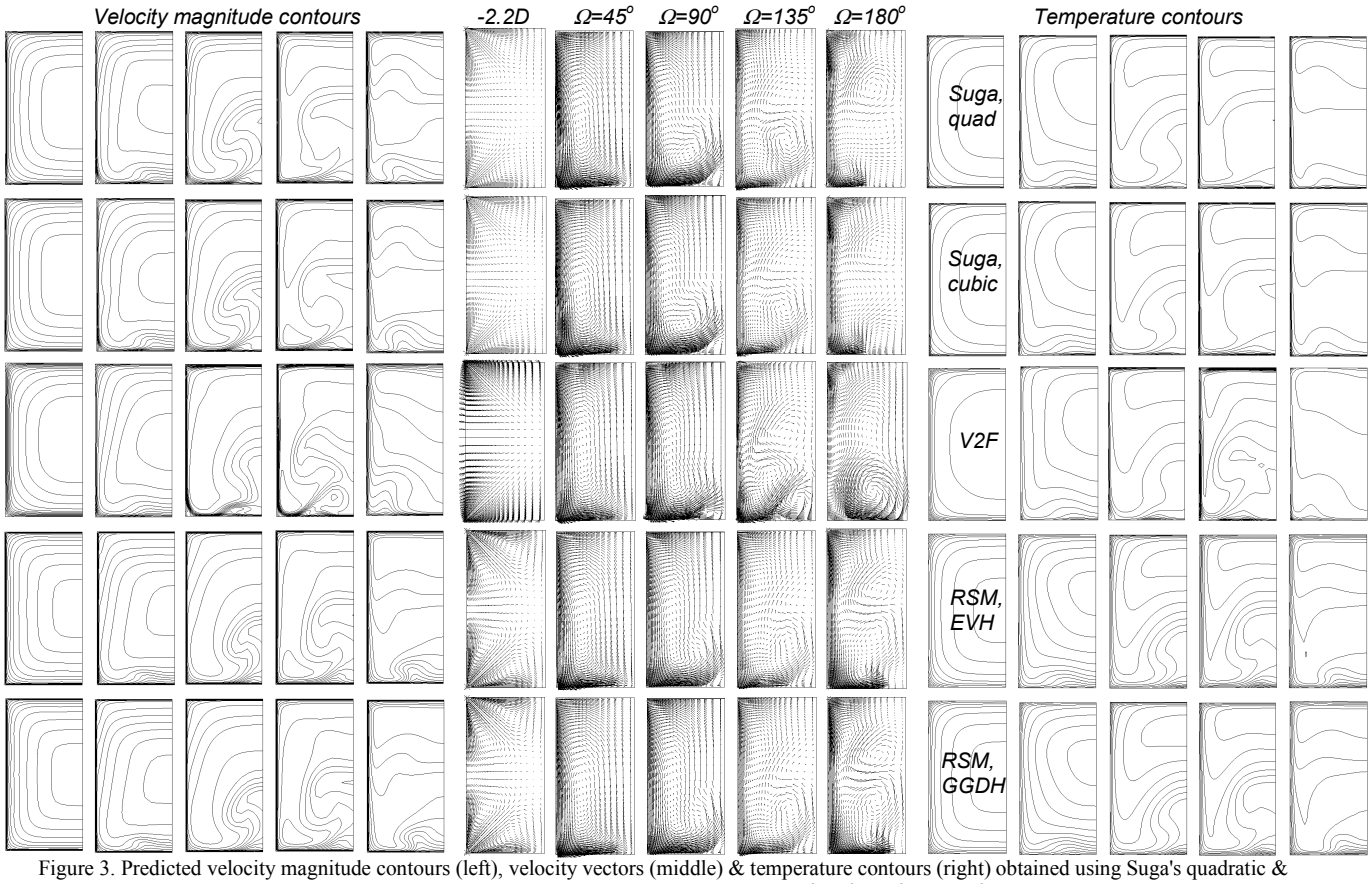

Figure 3. Predicted velocity magnitude contours (left), velocity vectors (middle) & temperature contours (right) obtained using Suga's quadratic & cubic model, V2F, RSM-EVH and RSM-GGDH (top to bottom, respectively) at -2.2*D*, 45°, 90°, 135° and 180°. Lower plot edge is the inner radius.

speed flow from the core towards the inner wall corner and later alongside the inner wall back towards the symmetry plane. This process brings cold high speed fluid near the inner wall which explains the double peak in the velocity profile and double dip in the temperature profile especially at 90°. The velocity vectors at -2.2*D* also show that, except V2F, all models have accounted for the anisotropy of turbulence in the inlet duct and predicted the turbulence induced secondary motion.

Conclusions

The flow and thermal fields in a square-sectioned 180°-bend were investigated using five turbulence models, namely Suga's quadratic and cubic low-Re k-ε, V2F k-ε, RSM-EVH and RSM-GGDH. All models managed to mimic the general flow and thermal patterns. The V2F-version used in this study seems, however, to need modifications and/or re-tuning of its coefficients to reduce its redistribution of turbulence energy. The RSM models performed best but Suga's two k-ε variants, despite their simplicity and relatively low computational effort, performed well and might be suitable for industrial applications.

Acknowledgments

The authors wish to acknowledge Lic. Engn. Olof Daunius for valuable discussions and his support and encouragements. This study is financed by the Swedish Agency for Innovation Systems (VINNOVA) and Volvo Car Corporation.

References

[1] Craft, T.J., Launder, B.E., and Suga, K., *Development and application of a cubic eddy viscosity models of turbulence*, Int. J. Heat and Fluid Flow, **17**, 1996, 108-115.

[2] Craft, T.J., Launder, B.E., and Suga, K., *Extending the applicability of eddy viscosity models through the use of deformation invariants and non-linear elements*, Proc. 5th Int. Symp. on Refined Flow Modelling and Turbulence Measurements, 1993, 125-132.

[3] Daly, B.J. and Harlow, F.H., *Transport equations in turbulence*, Phys. Fluids, **13**(11), 1970, 2634-2649.

[4] Durbin, P.A., *Separated flow computations with the k-ε-v² model*, AIAA Journal, **33**(4), 1995, 659-664.

[5] Etemad, S., Rokni, M., Sundén, B. and Daunius, O., *Analysis of Turbulent Flow and Heat Transfer in a Square-Sectioned U-Bend*, 4th Int. Symp. on Turbulence, Heat and Mass Transfer, Hanjalić, K., Nagano, Y. and Tummers, M., (Eds), Begell House Inc., 2003, 1171-1178.

[6] Etemad, S. and Sundén, B., *Prediction of Developing Turbulent Flow in a Rectangular-Sectioned Curved Duct*, HT-FED2004-56193, ASME Heat Transfer/Fluids Eng. Summer Conf., Charlotte, North Carolina, USA, 2004.

[7] Iaccarino, G., *Predictions of a turbulent separated flow using commercial CFD codes*, J. Fluids Eng., 123(4), 2001, 819-828.

[8] Johnson, R.W. and Launder, B.E., *Local Nusselt number and temperature field in turbulent flow through a heated square-sectioned U-bend*, Int. J. Heat and Fluid Flow, **6** (3), 1985, 171-180.

[9] Launder, B.E. and Sandham, N.D., (Eds.), *Closure strategies for turbulent and transitional flows*, Cambridge Univ. Press, 2002.

[10] Lien, F.S. and Leschziner, M.A., *A pressure-velocity solution strategy for compressible flow and its application to shock/boundary layer interaction using second-moment turbulence closure*, J. Fluids Eng., **115**, 1993, 717-725.

[11] Speziale, C.G., Sarkar, S., and Gatski, T.B., *Modelling the pressure-strain correlation of turbulence: an invariant dynamical system approach*, J. Fluid Mech., **227**, 1991, 245-272.

[12] STAR-CD, *Methodology, STAR-CD VERSION 3.2*, 2004, CD-Adapco Group.